

# Secondary fragmentation and relative biological effectiveness (RBE) study using Bridge SOI microdosimeter: Monte Carlo simulation

C. K. Ying<sup>1</sup> , M. Arif Efendi<sup>2</sup>, Susanna Guatelli<sup>3</sup>, Linh T. Tran<sup>3</sup> and David Bolst<sup>3</sup>

## Original Article

**Cite this article:** Ying CK, Arif Efendi M, Guatelli S, Tran LT, and Bolst D. (2024) Secondary fragmentation and relative biological effectiveness (RBE) study using Bridge SOI microdosimeter: Monte Carlo simulation. *Journal of Radiotherapy in Practice*. **23**(e1), 1–15. doi: [10.1017/S1460396923000420](https://doi.org/10.1017/S1460396923000420)

Received: 29 March 2023

Revised: 23 June 2023

Accepted: 13 July 2023

### Keywords:

Bridge silicon microdosimeter; Geant4 Monte Carlo simulation; microdosimetry; oxygen ion beam; relative biological effectiveness (RBE); TOPAS

### Corresponding author:

C. K. Ying; Email: [ckying7@usm.my](mailto:ckying7@usm.my)

<sup>1</sup>Department of Biomedical Imaging, Advanced Medical and Dental Institute, Universiti Sains Malaysia, Bertam, Penang, Malaysia; <sup>2</sup>Department of Nuclear Engineering and Engineering Physics, Faculty of Engineering, Universitas Gadjah Mada, Yogyakarta, Indonesia and <sup>3</sup>Centre for Medical Radiation Physics, University of Wollongong, Wollongong, NSW, Australia

## Abstract

**Introduction:** This work calculates the microdosimetric spectra and evaluates the relative biological effectiveness (RBE<sub>10</sub>) of oxygen and carbon ions using Monte Carlo simulation. This study presents a fast, reliable radiation field characterisation and accurate biological dose prediction tool in charged particle therapy for heavy-ion beams using the Bridge silicon-on-insulator (SOI) microdosimeter via Tool for Particle Simulation (TOPAS)-based simulations toolkit.

**Method:** The study used the TOPAS simulation to model the Bridge SOI microdosimeter and study its response to carbon beams with an energy of 290 MeV/u and oxygen beams with an energy of 345 MeV/u. Dose-mean lineal energy values ( $\overline{y_D}$ ) and RBE<sub>10</sub> values were evaluated using microdosimetric lineal energy spectra with the MKM model.

**Results and Conclusions:** The results demonstrate that oxygen ion beams have an advantage for cancer treatment as they provide higher RBE<sub>10</sub> values and occur at the same positions as the maximum physical dose (Bragg peak), compared to carbon ion beams. The study provides new understanding of RBE for carbon and oxygen ions, as well as the relationship between physical doses and RBE.

## Introduction

Charged particle therapy (CPT) with proton and carbon ions has been extensively used to treat various types of cancerous tumours [1,2]. Charged particles deposit the major part of their energy at the end of their range when penetrating water medium. This physical characteristic of the Bragg peak allows highly localised particle beams to deposit most of the energy on the tumour while minimising residual dose to surrounding normal tissues. Heavier ions such as carbon and oxygen ions have further advantages in treating deep-seated tumours compared with protons thanks to higher relative biological effectiveness (RBE) [3,4].

Proton and carbon ions are widely used in CPT worldwide. However, oxygen ions have recently gained more attention to be used in CPT [5]. Oxygen ions offer higher RBE, higher linear energy transfer (LET) and higher peak-to-entrance ratio compared to carbon ions. These characteristics are especially useful in treating hypoxic tumours [5–8]. The RBE of charged particles is not constant along their penetration depth. The RBE increases drastically at the Bragg peak position, but the maximum RBE value does not occur at the same depth as the maximum physical dose [9,10]. The evaluation of the RBE in the biological medium, especially around the Bragg peak, is crucial to deliver the required biological dose to the tumour.

Many types of microdosimeters can be used to measure microdosimetric and derive RBE using radiobiological models. Tissue equivalent proportional counters (TEPC) are the most common type of microdosimetry detectors, for measuring microdosimetric quantities to derive their RBE in CPT. Unfortunately, this technology has drawbacks which include, a low spatial resolution, which does not allow high spatial resolution microdosimetry measurements within the narrow region of the Bragg peak. Silicon-on-insulator (SOI) microdosimeters developed by the Centre for Medical Radiation Physics (CMRP) of the University of Wollongong in Australia were introduced to overcome the limitations of TEPCs. The large size of TEPCs is not ideal for the sharp dose profiles at the distal edge of Bragg peak and spatial resolution is limited. The SOI microdosimeter can measure the energy deposited by a mixed radiation field with high spatial resolution [11].

Monte Carlo simulation modelling particle transport in matter is widely used to characterise and improve radiation detectors. In this study, the Bridge SOI microdosimeter [11] was simulated using Tool for Particle Simulation (TOPAS) [12,13]. TOPAS is based on the Geant4 simulation toolkit [14]. It provides pre-built components (e.g. nozzles, geometry, dosimetry and imaging components) for users to simulate a wide variety of radiation beams and dosimeters

© The Author(s), 2024. Published by Cambridge University Press. This is an Open Access article, distributed under the terms of the Creative Commons Attribution licence (<http://creativecommons.org/licenses/by/4.0/>), which permits unrestricted re-use, distribution and reproduction, provided the original article is properly cited.

with no required extensive knowledge of C++ programming language. In this study, the TOPAS microdosimetric extension was used [15]. Pre-built geometry of the Bridge SOI microdosimeter is defined in the TOPAS microdosimetry extension, and the parameters necessary for the lineal energy scorer such as the sensitive volume radius, tissues-equivalent radius, position of the sensitive volume and mean path length were specified. The pre-built lineal energy scorer recorded the energy deposition of both the primary and secondary particles in the SVs of the detector. A detailed description of the lineal energy scorer can be found in Ref. [15].

To date, CPT has been extensively used to treat cancerous tumours. However, there has been limited discussion regarding microdosimetric quantities resulting from secondary fragments due to nuclear interactions and their biological effects, as well as the accurate prediction of RBE, particularly for novel oxygen ion species. Therefore, the study can play an important role in understanding the RBE values and accurate RBE prediction of oxygen ions and commissioning of RBE values used in treatment planning system and quality assurance.

TOPAS microdosimetric extension can simulate total and secondary fragment microdosimetric spectra, calculate microdosimetric parameters (e.g. frequency-mean lineal energy, dose-mean lineal energy) and determine the RBE<sub>10</sub> with the microdosimetric kinetic model (MKM). The simulation configuration of the TOPAS microdosimetric extension could adequately reproduce the experimental microdosimetric spectra of proton beams [15,16].

This work simulated and compared the microdosimetry spectra and evaluated RBE<sub>10</sub> produced in a water phantom by an oxygen ion beams with respect to a carbon ion beams. The results were compared to the experimental results available in literature, providing new understanding of RBE for carbon and oxygen ions, as well as the relationship between physical doses and RBE. This work also presents a possible, fast and reliable approach to evaluate RBE<sub>10</sub> value of carbon and oxygen ions using a Bridge SOI microdosimeter by means of TOPAS simulation.

## Materials and Method

### Microdosimetric quantities and RBE<sub>10</sub> calculation

Microdosimetric spectra are given in terms of the stochastic quantity, lineal energy,  $y$ , which is the fundamental microdosimetric quantity. The definitions of the microdosimetry quantities can be found in the International Commission on Radiation Units and Measurements (ICRU) Report 36 [17] and more details of the microdosimetry theory are described in the literature [18–20].  $y$  is the energy deposited in a single event in a micron-size sensitive volume (SV) per average chord length, given by:

$$y = \frac{\varepsilon}{\langle l \rangle} \quad (1)$$

where  $\varepsilon$  is the energy deposited for a single event in an SV with an average chord length  $\langle l \rangle$ .

The mean path length  $\langle l_{\text{path}} \rangle$  is used instead of the mean chord length in the TOPAS microdosimetric extension. The concept of  $\langle l_{\text{path}} \rangle$  was proposed by Bolst et al. [21] to suit the design of the Bridge SOI microdosimeter.

In this study,  $\langle l_{\text{path}} \rangle$  with a value of 10  $\mu\text{m}$  was used to represent the thickness of the silicon layer, considering the mean path of the charged particles when traversing the SV. The energy

depositions in the SV have to be converted to tissue-equivalent SV by using the conversion factor of 0.58 to get the equivalent energy deposition in tissues [21,22]. The frequency lineal energy spectrum,  $f(y)$ , for the generated primary and secondary charged particles, can be derived from the deposited energy spectrum. The dose lineal energy spectrum  $d(y)$  is given by:

$$d(y) = \frac{yf(y)}{\bar{y}_F} \quad (2)$$

where  $\bar{y}_F = \int_0^\infty yf(y)dy$  is the frequency-mean lineal energy. After obtaining the dose lineal energy  $d(y)$ , the dose-mean lineal energy  $\bar{y}_D$  can be calculated  $\bar{y}_D = \int_0^\infty yd(y)dy$ .

In this study, the modified MKM introduced by Kase et al. [18,19] was used to calculate the RBE, as previously done by Tran et al. [23]. This method is described as follows. The value of  $\bar{y}_D$  is used to determine the  $\alpha$  parameter in the Linear Quadratic Model (LQM), which describes the cell survival fraction in the radiation field of interest as:

$$S = \exp(-\alpha D - \beta D^2) \quad (3)$$

where  $\alpha = \alpha_0 + \frac{\beta}{\rho\pi r_d^2} y^*$ ,  $\beta$  is a parameter of the LQM survival curve (which assumes LET independence),  $\rho$  is the density of cell medium and can be assumed as water ( $\rho = 1 \text{ g/cm}^3$ ) and  $r_d$  is the radius of subcellular domain in the MKM.  $y^*$ , shown in Equation (4), is the saturation-corrected dose-mean lineal energy that takes into account the overkilling effect of excessive local energy deposition [20]:

$$y^* = \frac{y_0^2 \int_0^\infty (1 - \exp(-y^2/y_0^2))f(y)dy}{\int_0^\infty yf(y)dy} \quad (4)$$

The MKM parameters,  $y_0 = 150 \text{ keV}/\mu\text{m}$ ,  $\alpha_0 = 0.13 \text{ Gy}^{-1}$ ,  $\beta = 0.05 \text{ Gy}^{-2}$  and  $r_d = 0.42 \mu\text{m}$ , used in this study were the same as those adopted by Kase et al. [19], corresponding to the case of a human salivary gland tumour cell line. The RBE is defined as the ratio of the dose delivered with the reference radiation (200 kVp X-rays) to the dose that has to be delivered by the tested beam to obtain the same biological endpoint, e.g., the same cell survival  $S$ . The RBE for a 10% cell survival (RBE<sub>10</sub>) is expressed as:

$$\text{RBE}_{10} = \frac{2\beta D_{10,\text{ref}}}{\sqrt{\alpha^2 - 4\beta \ln(0.1)} - \alpha} \quad (5)$$

where  $D_{10,\text{ref}}$  (5 Gy) is the required dose by 200 kVp X-rays for a 10% cell survival.

### The Bridge SOI microdosimeter

In this study, the Monte Carlo simulation toolkit was used to model the Bridge SOI microdosimeter developed by CMRP [24–26]. The device is an array of 4,248 silicon sensitive volumes (SVs), organised in 59 rows and 72 columns, connected by bridging volumes of  $15 \times 20 \times 10 \mu\text{m}^3$  each. An individual SV's volume is  $30 \times 30 \times 10 \mu\text{m}^3$ . Bridging volumes have the same silicon characteristic of the SVs. The geometry of the detector is shown in Fig. 1. A more detailed description of the Bridge SOI microdosimeter can be found in literatures [15,23,26]. The device was characterised in detail and successfully tested with incident carbon, oxygen and nitrogen ions at Heavy Ion Medical Accelerator in Chiba (HIMAC), Japan by

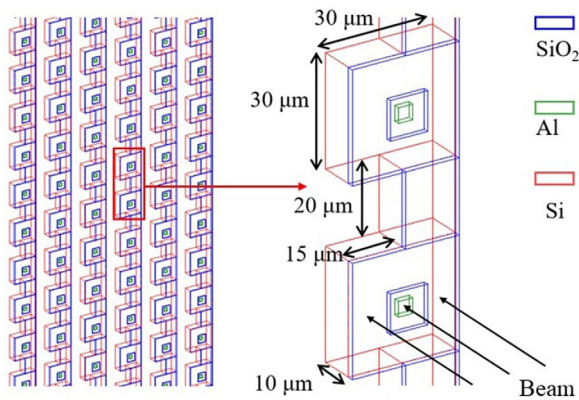


**Figure 1.** The geometry of the silicon-on-insulator detector (Source: Zhu et al. [15])

experiments and simulations using the Geant4 Monte Carlo simulation toolkit [9,16,23,26].

**TOPAS simulation**

The Bridge SOI microdosimeter was modelled in TOPAS version 3.6.0 (based on Geant4 10.06.p03), with its microdosimetry extension. Carbon ion beams were generated with an energy of 290 MeV/u, as this is the typical energy used in carbon ion therapy at HIMAC [27]. The energy distribution was considered Gaussian with an energy spread  $\sigma$  of 0.86 %. The beam spot size was simulated with  $\sigma = 11$  mm. The Bridge SOI microdosimeter was positioned at various depths (entrance of the phantom, at the Bragg peak, distal edge and tail regions) along the beam direction in the water phantom. The energy depositions of the primary particle and all its correlated secondary particles are scored. At the end of simulation of each run, the energy deposition event scores are processed by analysis toolkit and the microdosimetric spectra are obtained.

Since the SVs in Bridge SOI microdosimeter are made of silicon materials, a tissue-equivalent conversion factor of 0.58 is needed to convert the simulated energy in the SVs to a tissue-equivalent material [21,22]. The tissue-equivalent conversion factor was obtained by simulating the silicon microdosimeter and by irradiating it with 290 MeV/u  $^{12}\text{C}$  beam at different depths in a water phantom. The silicon microdosimeter was then replaced with tissue-equivalent material (straited muscle) at the same depth as the silicon microdosimeter, simulating the tissues-equivalent material with same energy. However, the size of the tissue SV was varied to obtain the same energy deposition spectrum as the silicon SV. In this case, the tissue-equivalent conversion factor is defined as the ratio of the length of the silicon SV to the length of the tissue SV.

Study by Bolst et al. [22] shows that the calculated correction factors can determine  $\text{RBE}_{10}$  with good agreement based on TEPC

measurements. The maximum difference was about 5% when comparing the simulated silicon cylinder SV's response to the simulated tissue sphere SV's response. More detail on the conversion factor calculation can be found in Bolst et al. [21,22]. As suggested by Zhu et al. [15] the lower threshold linear energy was set to 0.5 keV/ $\mu\text{m}$  considering the detection threshold of the detector was 0.3–0.4 KeV/ $\mu\text{m}$  and  $^{12}\text{C}$  experimental spectra starting from about 0.5 KeV/ $\mu\text{m}$  at the entrance of the phantom. The depth dose distribution in a water phantom was also simulated; the dose distribution was scored along the beam axis in a cylinder of 2.5 cm diameter and 30 cm depth.

The simulations were repeated using an oxygen ion beam with energy of 345 MeV/u. This corresponds to a range of approximately 160 mm in water which is similar to the case of the carbon ion beam under investigation. All simulations were performed with  $10^6$  track histories [28,29] while  $10^7$  track histories were simulated at the distal tail of the Bragg peak. The G4HadronPhysicsQGSP\_BIC\_HP and G4HadronElasticPhysicsHP were used to describe the inelastic and elastic interactions, the G4EmStandardPhysics\_Option\_4 described electromagnetic interactions, the G4IonBinarCascadedPhysics described hadronic interactions of ions. For optimal simulation time but not sacrificing the accuracy of simulation results, the *CutsPerRegion* functionality was used, to avoid the tracking of secondary electrons, which cannot reach and deposit energy in the detector. The electron production cut was set to 1  $\mu\text{m}$  in the region surrounding the microdosimeter. Outside this region, the default cut value in the water phantom was set equal to 2 mm.

To further investigate the  $\text{RBE}_{10}$  distribution by means of TOPAS simulation, the cylindrical mini-Tissue Equivalent Proportional Counter (mini-TEPC) developed by Istituto Nazionale di Fisica Nucleare (INFN) was also simulated. This mini-TEPC has a cylindrical SV of 0.9 mm diameter, surrounded by 0.35 mm thick A-150-cathod wall and insulator with 0.2 mm thick aluminium sleeve. The mini-TEPC was able to collect accurate data in Bragg peak region due to its small size [30]. The geometry of the mini-TEPC is shown in Fig. 2. and more details can be found in the Ref. [31]. To compare  $\text{RBE}_{10}$  distributions between mini-TEPC and Bridge SOI microdosimeter, the simulations were repeated and the Bridge SOI microdosimeter was substituted with mini-TEPC. These adopted the same simulation configurations and energies.

**Results and Discussion**

**Dose-mean linear energy and  $\text{RBE}_{10}$**

Fig. 3 shows the relative absorbed dose in the water phantom for both 290 MeV/u  $^{12}\text{C}$  and 345 MeV/u  $^{16}\text{O}$  beams, normalised to per incident particle. At the entrance, at 2 mm depth from the surface of the phantom, the dose deposition for the  $^{16}\text{O}$  ion beam was

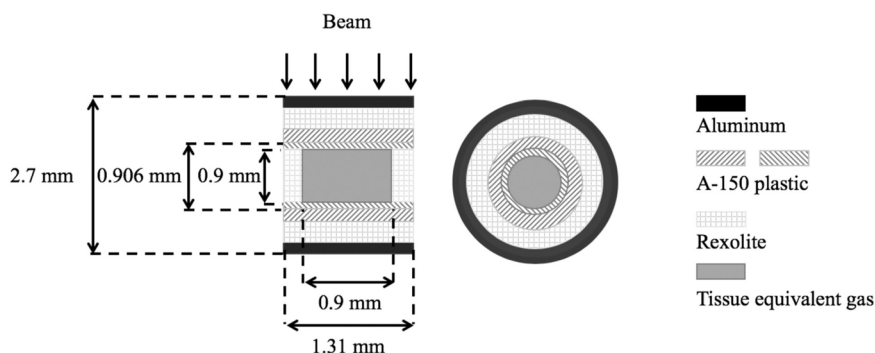


**Figure 2.** The geometry of the mini-tissue equivalent proportional counters (Source: Zhu et al. [15])

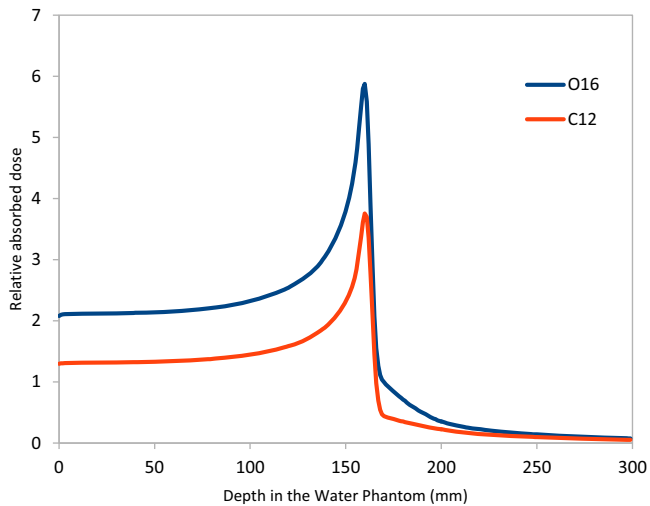
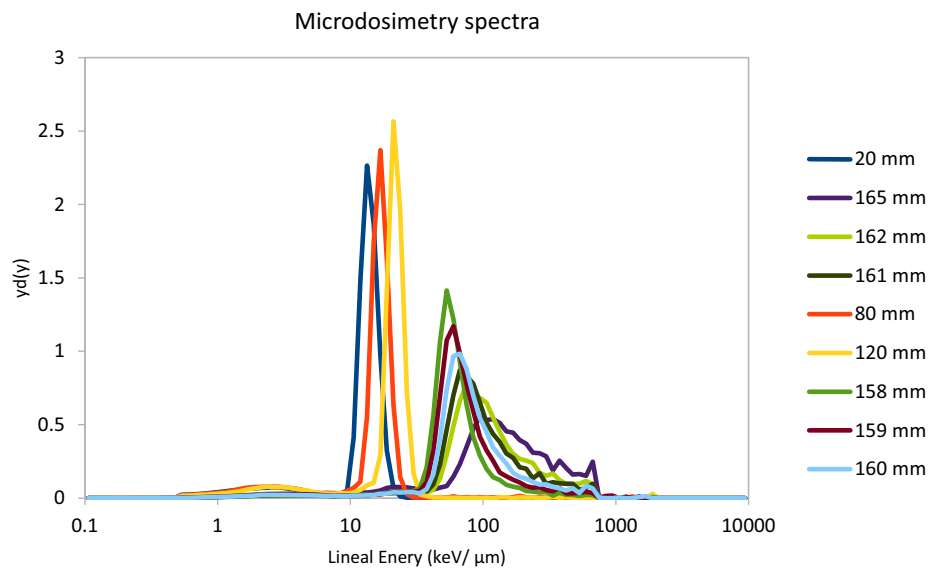


**Figure 3.** Relative absorbed dose profile in water phantom per incident particle for 290 MeV/u  $^{12}\text{C}$  (red) and 345 MeV/u  $^{16}\text{O}$  (blue) ion beams

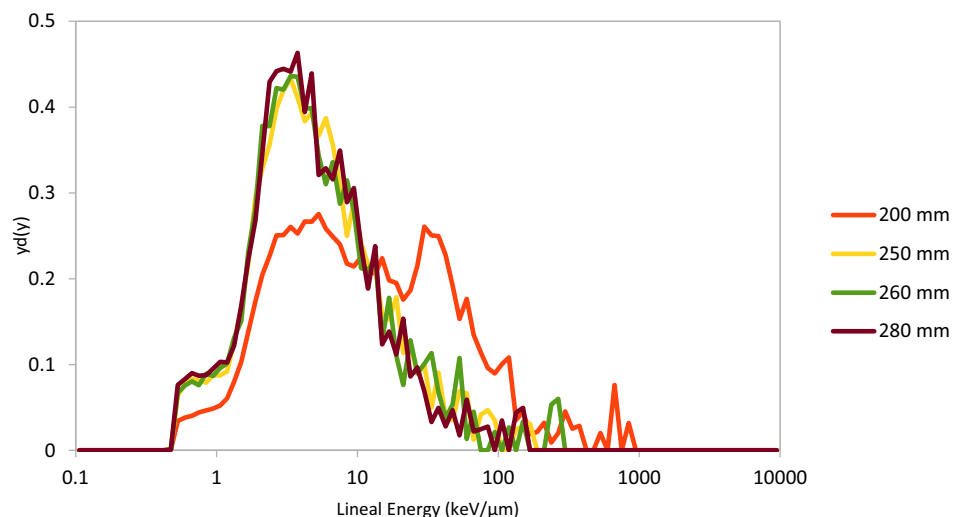
about 60% higher than the case of  $^{12}\text{C}$  ions. Both  $^{16}\text{O}$  and  $^{12}\text{C}$  ions deposited their maximum dose approximately at 160 mm depth from the surface of the phantom, i.e., at the Bragg peak. At the Bragg peak, the  $^{16}\text{O}$  ion beam produces approximately 56% higher dose deposition than the  $^{12}\text{C}$  ion beam. At the distal part of the Bragg peak (2 mm beyond the Bragg peak), the  $^{16}\text{O}$  ion beam still produces 45% higher dose deposition than the  $^{12}\text{C}$  ion beam. The dose at the distal edge should be taken into consideration because organs-at-risk may be located at the distal edge.

Fig. 4 shows the simulated microdosimetric,  $yd(y)$ , spectra plotted as a function of lineal energy,  $y$ , obtained with the modelling of the Bridge SOI microdosimeter for  $^{12}\text{C}$  ions, at depths of 20, 80, 120, 158, 159, 160, 161, 162 and 165 mm in a water phantom. Fig. 5 shows the microdosimetric spectra at the distal part of the Bragg peak at 200, 250, 260 and 280 mm.

The highest simulated  $yd(y)$  value of 2.57 can be observed at a lineal energy of approximately 21 keV/ $\mu\text{m}$ , at a depth of 120 mm. As expected, lineal energy values are observed to increase when the beam penetrates deeper into the water, this is because of increased



**Figure 4.** Simulated microdosimetric spectra for a 290 MeV/u  $^{12}\text{C}$  beam at 20, 80, 120, 158, 159, 160, 161, 162 and 165 mm depth in water



**Figure 5.** Simulated microdosimetric spectra for a 290 MeV/u  $^{12}\text{C}$  beam at 200, 250, 260 and 280 mm depth in water

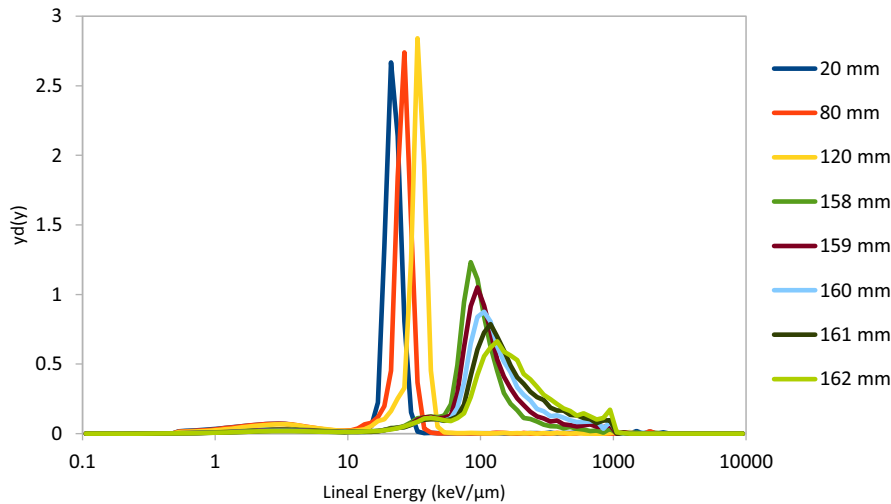


**Figure 6.** Simulated microdosimetric spectra for a 345 MeV/u  $^{16}\text{O}$  beam at 20, 80, 120, 158, 159, 160, 161 and 162 mm depth in water

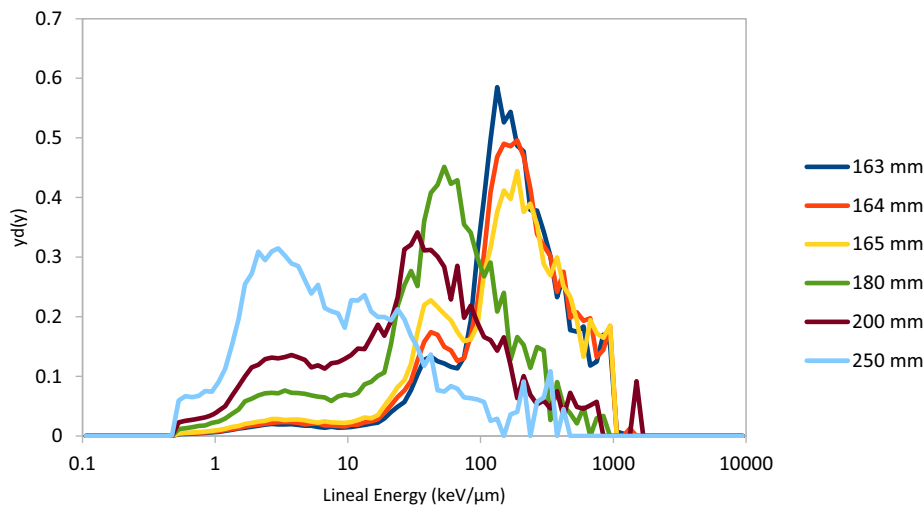


**Figure 7.** Simulated microdosimetric spectra for a 345 MeV/u  $^{16}\text{O}$  beam at 163, 164, 165, 180, 200 and 250 mm depth in water

LET of incident ions and also contribution from secondary fragmentations generated along the penetration depth.

Fig. 6 shows the simulated microdosimetric spectra obtained with the modelling of the Bridge SOI microdosimeter for  $^{16}\text{O}$  ions, at depths of 20, 80, 120, 158, 159, 160, 161 and 162 mm. Fig. 7 shows the microdosimetric spectra at the distal part of the Bragg peak, at 163, 164, 165, 180, 200 and 250 mm. Similar to the case of  $^{12}\text{C}$  ions, the highest  $y_d(y)$  value of 2.84 can be observed at a lineal energy of approximately 34 keV/ $\mu\text{m}$ , at a depth of 120 mm. The lineal energy values are observed to increase also after the Bragg peak at the downstream region between 163 and 165 mm.

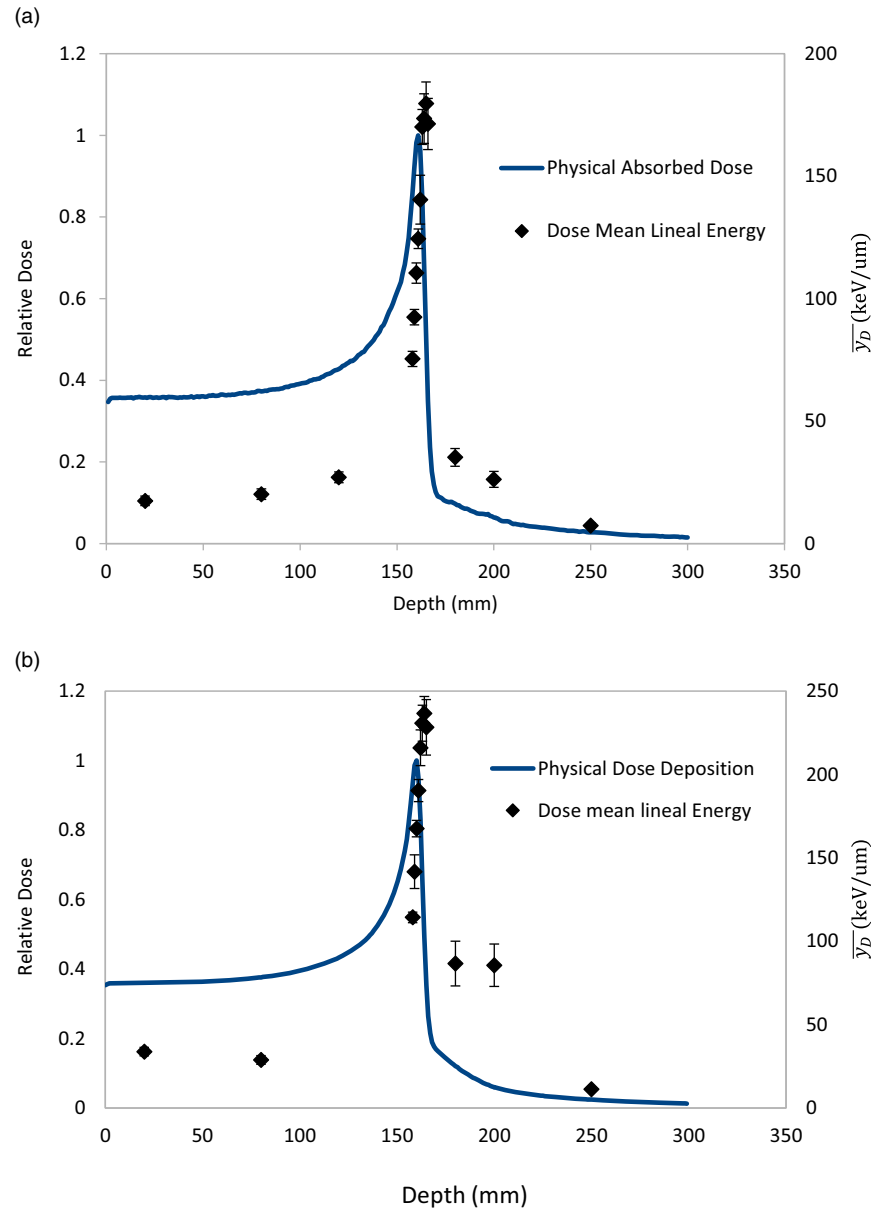
It could be observed that Figs. 5 and 7 has a higher uncertainty due to its location at the distal part of the Bragg peak. This is because only secondary particles contributed to the energy depositions, originating from nuclear interactions that, being rare events but high-energy deposition, have a negative impact on uncertainty and strong impact the value of  $\bar{y}_D$  [29].

Fig. 8a and 8b show the dose-mean lineal energy values,  $\bar{y}_D$ , obtained with the simulated Bridge SOI microdosimeter in a water phantom for  $^{12}\text{C}$  and  $^{16}\text{O}$ , respectively. The  $\bar{y}_D$  values for  $^{12}\text{C}$  were

approximately 17 keV/ $\mu\text{m}$  at the entrance, 75 keV/ $\mu\text{m}$  at 2 mm before the Bragg peak and increasing to approximately 110 keV/ $\mu\text{m}$  right at the Bragg peak. The maximum  $\bar{y}_D$  value was approximately 180 keV/ $\mu\text{m}$  and occurred 5 mm beyond the maximum dose at the Bragg peak, then decreasing to approximately 7 keV/ $\mu\text{m}$  in the tail region, at 250 mm depth. These values, obtained with TOPAS-based simulations, are compared to the measurement values by Tran et al. [9], performed in Gunma University heavy-ion medical centre using a 290 MeV/u  $^{12}\text{C}$  by using percentage difference, PD, as defined in Equation (6), where  $Exp$  is the quantity value from measurement and  $Sim$  in the value from simulation.

$$PD = \frac{(Sim - Exp)}{Exp} \times 100\% \quad (6)$$

Table 1 shows the comparison between the  $\bar{y}_D$  values measured by Tran et al. [9] and  $\bar{y}_D$  values in this study for  $^{12}\text{C}$ . The differences observed between simulations and measurements could be explained by the fact that the LET increases rapidly at the end



**Figure 8.** Simulated  $\bar{y}_D$  profile obtained with the Bridge SOI microdosimeter for (a) 290 MeV/u  $^{12}\text{C}$  and (b) 345 MeV/u  $^{16}\text{O}$  ion beam

**Table 1.** Comparison of the entrance  $\bar{y}_D$  value and maximum  $\bar{y}_D$  value for  $^{12}\text{C}$  between measurement by Tran et al. [9] and simulation in this study

	Entrance (keV/ $\mu\text{m}$ )	Maximum $\bar{y}_D$ value (keV/ $\mu\text{m}$ )	Position maximum $\bar{y}_D$ value
Tran et al. [9]	13	141	3 mm beyond Bragg peak
This study	17	180	5 mm beyond Bragg peak
PD	30%	27%	

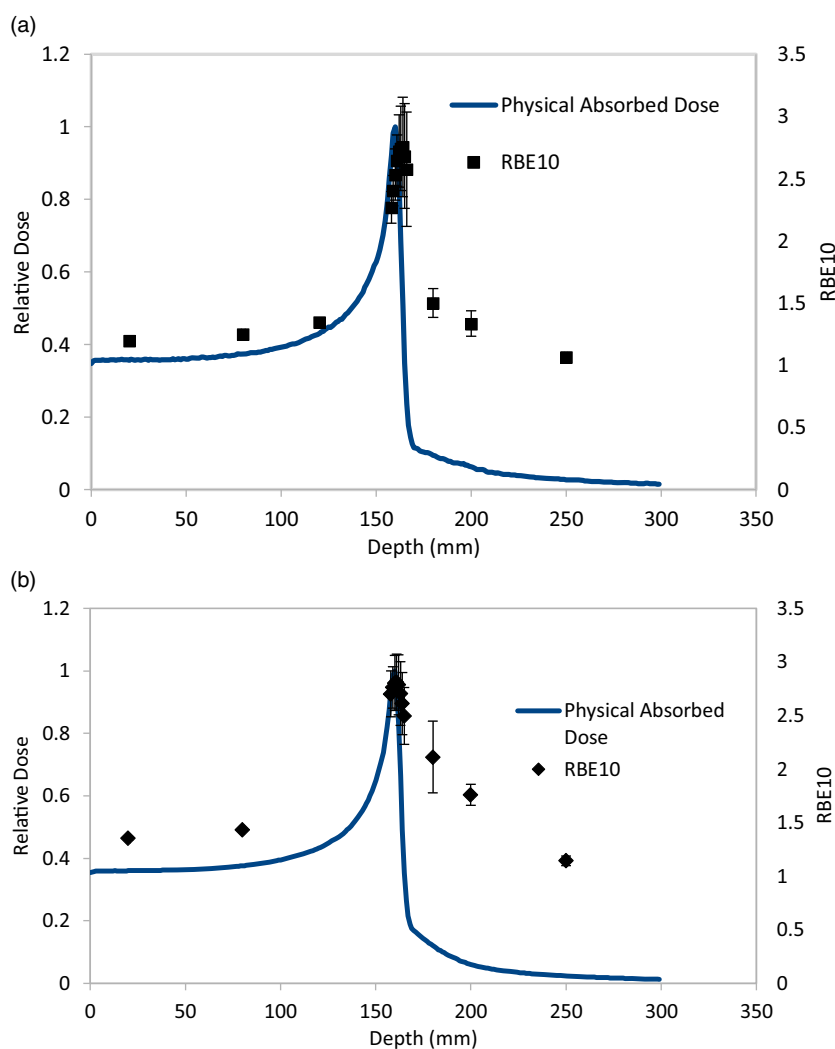
of a carbon ion's range, with a sharp dose gradient. This implies a very small change in depth can change the  $\bar{y}_D$  value drastically. Further, while a pristine mono-energetic beam was simulated, a ripple filter was used to broaden the range of the measured carbon ions beam. Please take into consideration that these simulations were not meant to model the experimental scanning beamline in Gunma University. Thus, the comparison shown in the Table 1 is just meant to provide a general idea of the capabilities of the

TOPAS-based simulations and not to provide a direct comparison with the measurement values.

The  $\bar{y}_D$  values for  $^{16}\text{O}$  were approximately 34 keV/ $\mu\text{m}$  at the entrance, which is twice greater than  $^{12}\text{C}$ . The  $\bar{y}_D$  value increases to approximately 114 keV/ $\mu\text{m}$  at 158 mm depth and approximately 168 keV/ $\mu\text{m}$  at the Bragg peak. Similar to  $^{12}\text{C}$  ions, the maximum  $\bar{y}_D$  value of 237 keV/ $\mu\text{m}$  for  $^{16}\text{O}$  ions can be observed at the distal part of the Bragg peak, specifically at a depth of 164 mm, which is

**Table 2.** Comparison of relative biological effectiveness values for  $^{12}\text{C}$  and  $^{16}\text{O}$  ions

Depth/mm	20	80	120	158	159	160	161	162	163
RBE <sub>10</sub> $^{12}\text{C}$ (Standard deviation)	1.20 (0.01)	1.25 (0.02)	1.35 (0.02)	2.27 (0.13)	2.40 (0.12)	2.53 (0.21)	2.65 (0.21)	2.72 (0.29)	2.74 (0.34)
RBE <sub>10</sub> $^{16}\text{O}$ (Standard deviation)	1.35 (0.02)	1.43 (0.01)	1.59 (0.02)	2.70 (0.21)	2.76 (0.19)	2.80 (0.26)	2.81 (0.26)	2.78 (0.28)	2.70 (0.30)
Depth/mm	164	165	180	200	250				
RBE <sub>10</sub> $^{12}\text{C}$ (Standard deviation)	2.75 (0.40)	2.68 (0.42)	1.50 (0.12)	1.33 (0.10)	1.06 (0.04)				
RBE <sub>10</sub> $^{16}\text{O}$ (Standard deviation)	2.61 (0.29)	2.50 (0.27)	2.11 (0.34)	1.76 (0.10)	1.14 (0.05)				

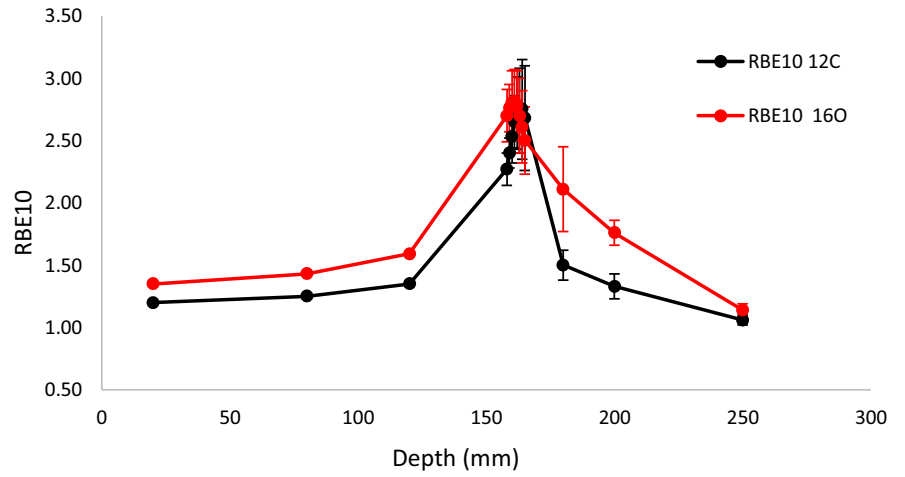
**Figure 9.** Simulated RBE<sub>10</sub> distribution obtained with the Bridge SOI microdosimeter for (a) 290 MeV/u  $^{12}\text{C}$  and (b) 345 MeV/u  $^{16}\text{O}$  ion beam

slightly behind the Bragg peak. The  $\bar{y}_D$  value then decreases to approximately 11 keV/ $\mu\text{m}$  in the tail region, at 250 mm depth in the water phantom.

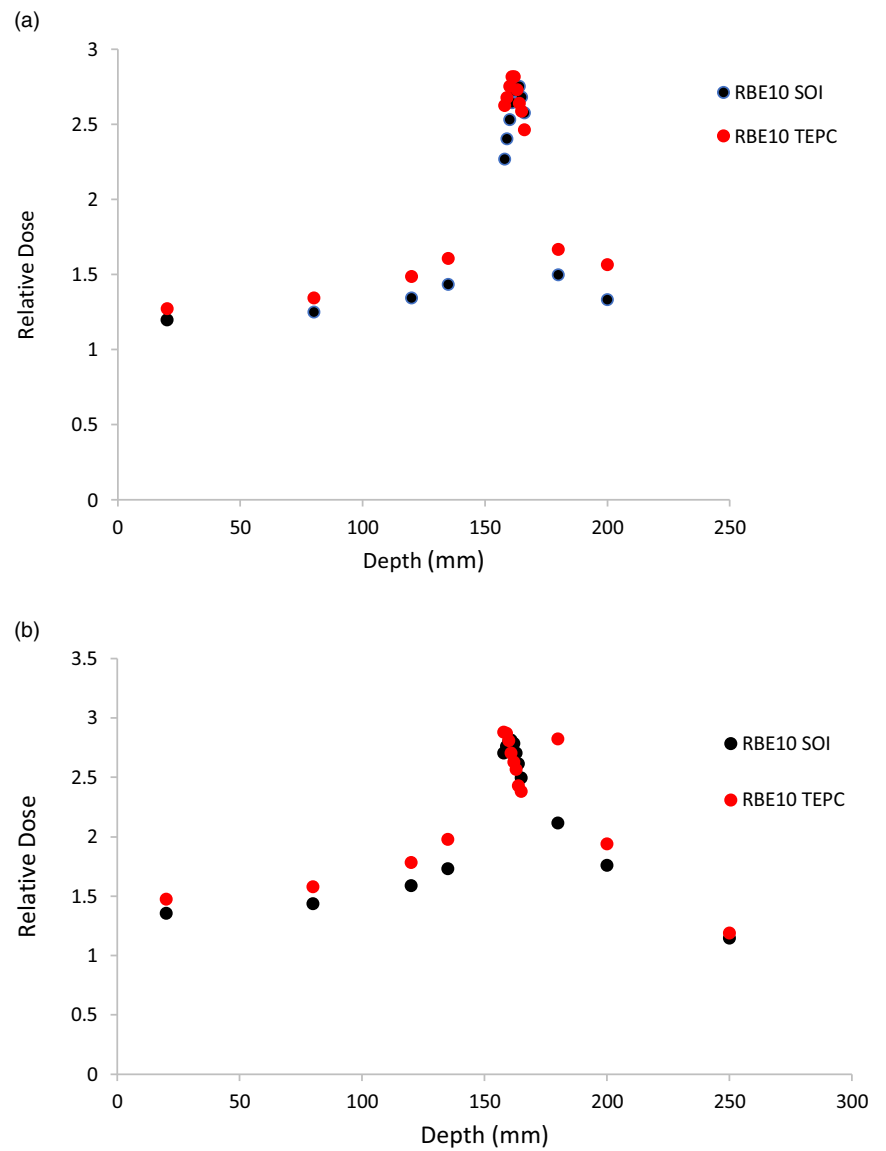
#### RBE<sub>10</sub> calculation with MKM

Table 2 shows the derived RBE<sub>10</sub> values for  $^{12}\text{C}$  and  $^{16}\text{O}$  ions and Fig. 9a and 9b show the derived RBE<sub>10</sub> distribution in the water

phantom, obtained through simulations using the Bridge SOI microdosimeter for  $^{12}\text{C}$  and  $^{16}\text{O}$  ions, respectively. The RBE<sub>10</sub> value for  $^{12}\text{C}$  ions at the entrance is approximately 1.25 (at 20 mm), increasing to 2.53 at the Bragg peak (depth 160 mm). The maximum RBE<sub>10</sub> value of approximately 2.75 occurs at 164 mm, which is 4 mm after the maximum dose at the Bragg peak. The position of the maximum RBE<sub>10</sub> obtained for  $^{12}\text{C}$  ions in this study is different from the one obtained experimentally by Tran et al. [9],



**Figure 10.** Comparison of simulated  $RBE_{10}$  profile obtained with the Bridge SOI microdosimeter for 290 MeV/u  $^{12}\text{C}$  and 345 MeV/u  $^{16}\text{O}$  ion beams



**Figure 11.** Simulated  $RBE_{10}$  distribution obtained with the Bridge SOI microdosimeter and mini-TEPC for (a) 290 MeV/u  $^{12}\text{C}$  and (b) 345 MeV/u  $^{16}\text{O}$  ion beam

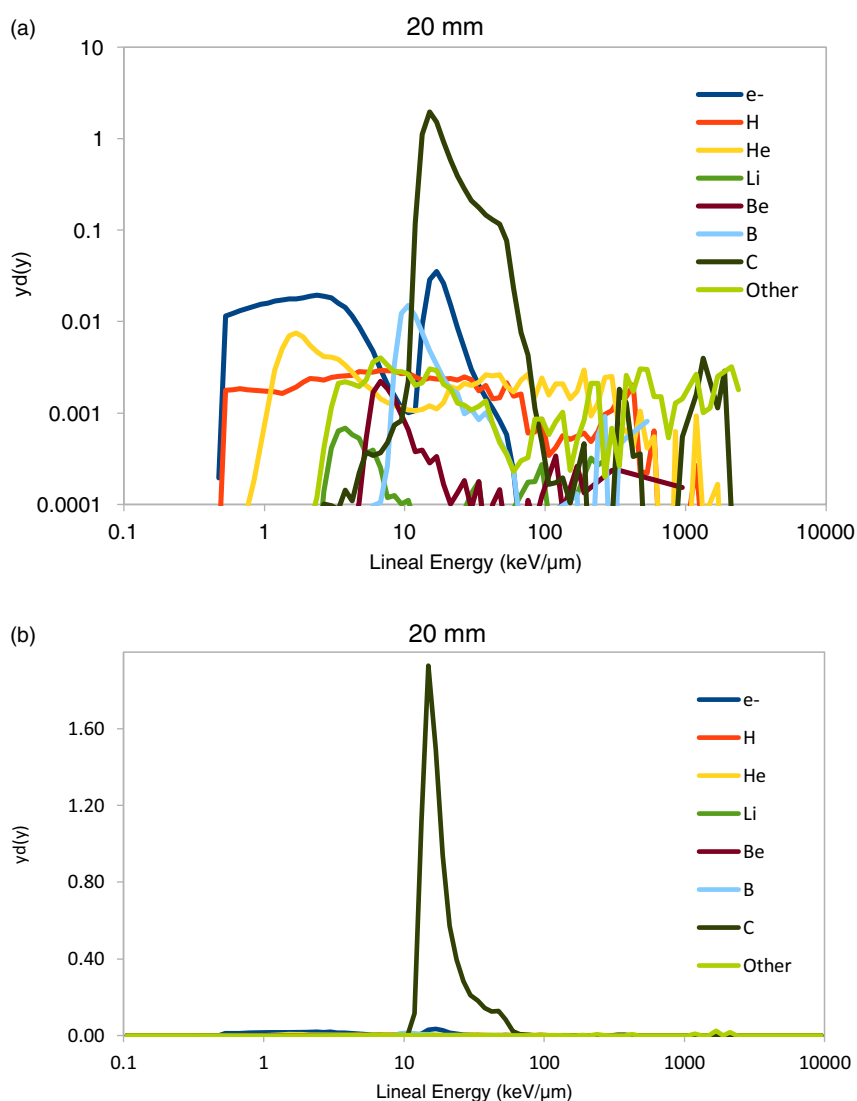


**Figure 12.** Secondary fragments contributing to the microdosimetric spectrum obtained with the Bridge SOI micropdosimeter for 290 MeV/u  $^{12}\text{C}$  ion beam set at 20 mm depth (a) log-log scale (b) semi-log scale

who reported the maximum  $\text{RBE}_{10}$  value at Bragg peak. In the tail region, at 250 mm depth in water, the  $\text{RBE}_{10}$  value decreases to approximately 1.1.

The  $\text{RBE}_{10}$  value for  $^{16}\text{O}$  ions at the entrance is 1.35 (at 20 mm), and the maximum  $\text{RBE}_{10}$  value is 2.81 at 161 mm, which is 1 mm after the maximum dose at the Bragg peak. At the distal part of the Bragg peak, the  $\text{RBE}_{10}$  value decreases slightly to 2.70 at 163 mm. In the tail region (250 mm depth in the water), similarly to the case of  $^{12}\text{C}$  ions, the  $\text{RBE}_{10}$  value of  $^{16}\text{O}$  decreases to approximately 1.1.

Fig. 10 shows the comparison of simulated  $\text{RBE}_{10}$  between  $^{12}\text{C}$  and  $^{16}\text{O}$  ion beams along the penetration depths in the water phantom obtained simulating the Bridge SOI microdosimeter. Overall, the  $\text{RBE}_{10}$  values for  $^{16}\text{O}$  ions were higher than the case of

$^{12}\text{C}$  ions at the entrance, before the Bragg peak and in the distal part of the Bragg peak. The maximum  $\text{RBE}_{10}$  value of  $^{12}\text{C}$  and  $^{16}\text{O}$  was 2.75 and 2.81, respectively. The maximum  $\text{RBE}_{10}$  value for  $^{16}\text{O}$  was reached earlier in depth (161 mm) than in the case of  $^{12}\text{C}$  (164 mm). At the tail region 250 mm, both  $^{12}\text{C}$  and  $^{16}\text{O}$  have approximately the same  $\text{RBE}_{10}$  value of 1.1.

Fig. 11a and 11b show the comparison of  $\text{RBE}_{10}$  profile obtained simulating the Bridge SOI microdosimeter and the mini-TEPC for 290 MeV/u  $^{12}\text{C}$  ion beam and 345 MeV/u  $^{16}\text{O}$  ion beam, respectively. Overall, the  $\text{RBE}_{10}$  values obtained simulating the mini-TEPC were slightly higher than the case of Bridge SOI microdosimeter at the entrance, before the Bragg peak and in the distal part of the Bragg peak. The discrepancy could be due to the difference in geometry of the SVs in the two detectors, and

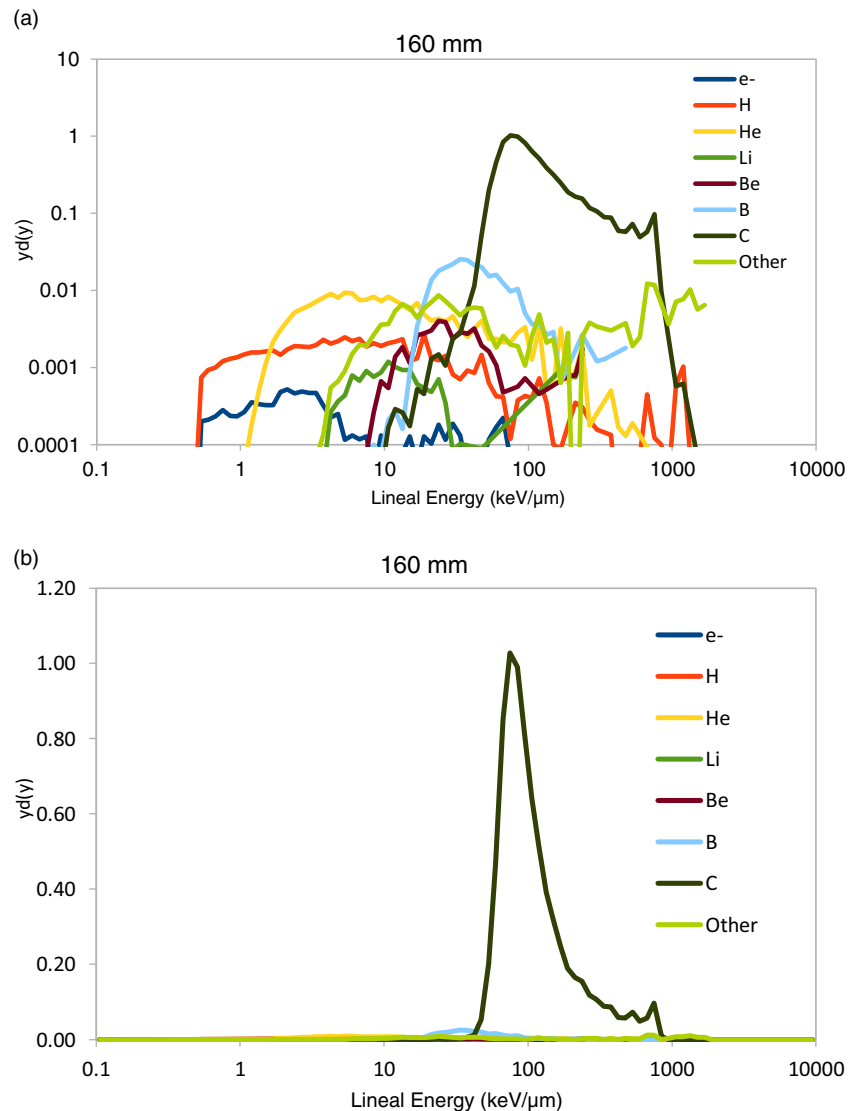


**Figure 13.** Secondary fragments contributing to the microdosimetric spectrum obtained with the Bridge SOI microdosimeter for 290 MeV/u  $^{12}\text{C}$  ion beam set at 160 mm depth (a) log-log scale (b) semi-log scale

the additional events caused by the delta rays produced in the structural materials of the mini-TEPC. The Bridge SOI microdosimeter has advantages due to its small sensitive volume size allowing it to calculate microdosimetric quantities with high spatial resolution. It also does not require gas flow as a mini-TEPC does.

The highest  $\text{RBE}_{10}$  value of  $^{12}\text{C}$  ion beam was 2.8 obtained with mini-TEPC at 161 mm (Bragg peak region), which is 1 mm after the maximum dose at the Bragg peak. In comparison with the Bridge SOI microdosimeter, which is 4 mm after the maximum dose at the Bragg peak with the  $\text{RBE}_{10}$  value of 2.7. The highest  $\text{RBE}_{10}$  value of  $^{16}\text{O}$  ion beam obtained simulating the mini-TEPC was 2.9, which occurred at 158 mm (Bragg peak region), which is 2 mm before the maximum dose at the Bragg peak. In comparison with the Bridge SOI microdosimeter at 161 mm, which is 1 mm after the maximum dose at the Bragg peak with the  $\text{RBE}_{10}$  value of 2.8.

#### *Contribution of secondary fragments to the microdosimetric spectra*

Figs. 12–14 show the different secondary fragments contributing to the microdosimetric spectra obtained with the Bridge SOI microdosimeter for 290 MeV/u  $^{12}\text{C}$  ion beam at 20, 160 and 250 mm depth in a water phantom, in logarithmic scale and semi-logarithmic scale plots, calculated by means of TOPAS. At the entrance at 20 mm, the main contribution to the spectrum was mainly due to carbon ion (96.3%), followed by electron (1.7%) at lineal energy range of 10–100 keV/ $\mu\text{m}$ . Contributions from other secondary fragments were almost negligible. Their presence in the semi-log plot shown in Fig. 12b, indeed, could barely be noticed.

At the Bragg peak at 160 mm, the main contribution to the spectrum was due to carbon ion (95.8%), followed by secondary fragments with  $Z > 6$  (2.8%) and boron (0.6%) at the higher lineal

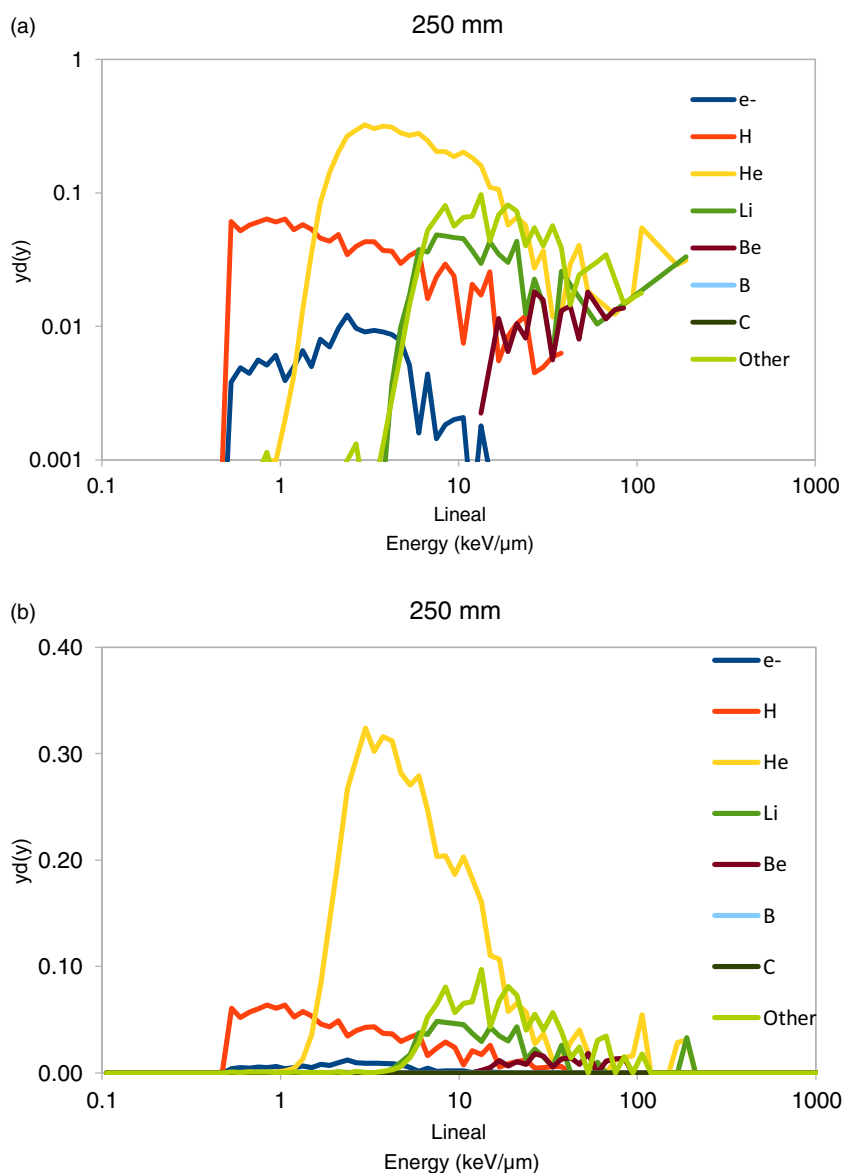


**Figure 14.** Secondary fragments contributing to the microdosimetric spectrum obtained with the Bridge SOI microdosimeter for 290 MeV/u  $^{12}\text{C}$  ion beam set at 250 mm depth (a) log-log scale (b) semi-log scale

energy range of 100–1,000 keV/μm. Contribution from lighter fragments dominated at the lower lineal energy range of 1–10 KeV/μm, which is helium (62.8%), followed by hydrogen (21.8%), secondary fragments with  $Z > 6$  (8.1%), electron (3.4%) and lithium (2.9%). Contribution from beryllium, boron and carbon could be observed with less than 1%.

At the tail region at 250 mm, the microdosimetric spectrum was produced by the secondary mixed radiation field only, mainly dominated by helium (63.2%), followed by secondary fragments with  $Z > 6$  (14.3%), hydrogen (11.3%) and lithium (7.4%) at lineal energy range of 1–100 keV/μm. Contribution from secondary electrons and beryllium could also be observed. The contribution from boron and carbon was not observed.

Fig. 15–17 show different secondary fragments contributing to the microdosimetric spectrum obtained with the Bridge SOI microdosimeter for 345 MeV/u  $^{16}\text{O}$  ion beam at 20, 160 and 250 mm depth in a water phantom, calculated by means of TOPAS. At the entrance at 20 mm depth in the water phantom, the main contribution to the spectrum was due to secondary fragments with  $Z > 6$  (97%), followed by secondary electrons (1.8%), carbon (0.5%), helium (0.3%) and hydrogen (0.3%) at lineal energy range of 10–100 keV/μm.

At the Bragg peak region at 160 mm depth in the water phantom, the main contribution to the spectrum was only due to secondary fragments with  $Z > 6$  (99%) at the lineal range of 100–1,000 keV/μm. The contribution from electron, hydrogen,

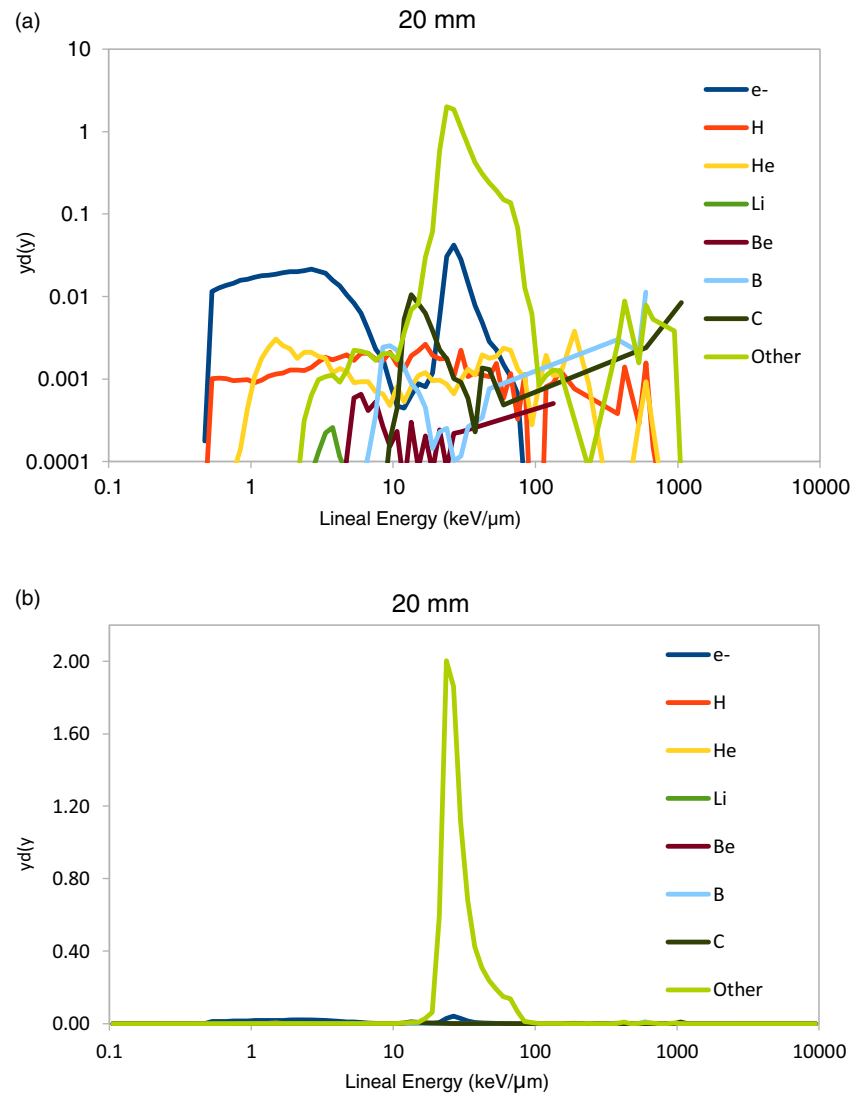


**Figure 15.** Secondary fragments contributing to the microdosimetric spectrum obtained with the Bridge SOI micropdosimeter for 345 MeV/u  $^{16}\text{O}$  ion beam set at 20 mm depth (a) log-log scale (b) semi-log scale

lithium, beryllium, helium, carbon and boron fragments was less than 1% and could only be observed in the log-log scale representation in Fig. 16a.

At the tail region, the microdosimetric spectrum is similar to the  $^{12}\text{C}$  beam with helium fragments as the main contribution to the spectrum (45.3%), followed by other secondaries were all fragments with  $Z > 6$  (24.4%), boron (11.3%), hydrogen (9.9%), beryllium (4.5%), lithium (2.6%), electron, (1.9%) and carbon (0.1%) at lineal energy range of 1–100 KeV/ $\mu\text{m}$ .

## Conclusion

Monte Carlo simulations have been widely used to study the various ion beams' mixed radiation field and to model microdosimeter detectors when irradiated with ion beams. This work presented a comparison of the  $\text{RBE}_{10}$  and dose-mean lineal energy ( $\bar{y}_D$ ) produced by oxygen ions and by carbon ions in a water

phantom. This study was carried out using TOPAS, a Geant4-based Monte Carlo simulation toolkit. Oxygen ions are currently considered a potential alternative to carbon ions because oxygen ions have less lateral scattering and higher LET associated with higher RBE, which translates to better treatment effectiveness. Therefore, oxygen ions have been proposed as an alternative to carbon ions in charged particle therapy for treatment of hypoxic tumours [5–8].

This work showed that  $\bar{y}_D$  values at the entrance for carbon and oxygen ion beams are about and 34 keV/ $\mu\text{m}$ , respectively. The maximum  $\bar{y}_D$  values for both carbon ions and oxygen ions, respectively 180 and 237 keV/ $\mu\text{m}$ , occurred slightly behind the maximum physical dose. The simulated maximum  $\text{RBE}_{10}$  value of carbon ions also occurred slightly after the maximum physical dose. This result is slightly different from the measurement value found in the literature though, occurring at the same position as maximum physical dose [9]. On the other hand, the simulated

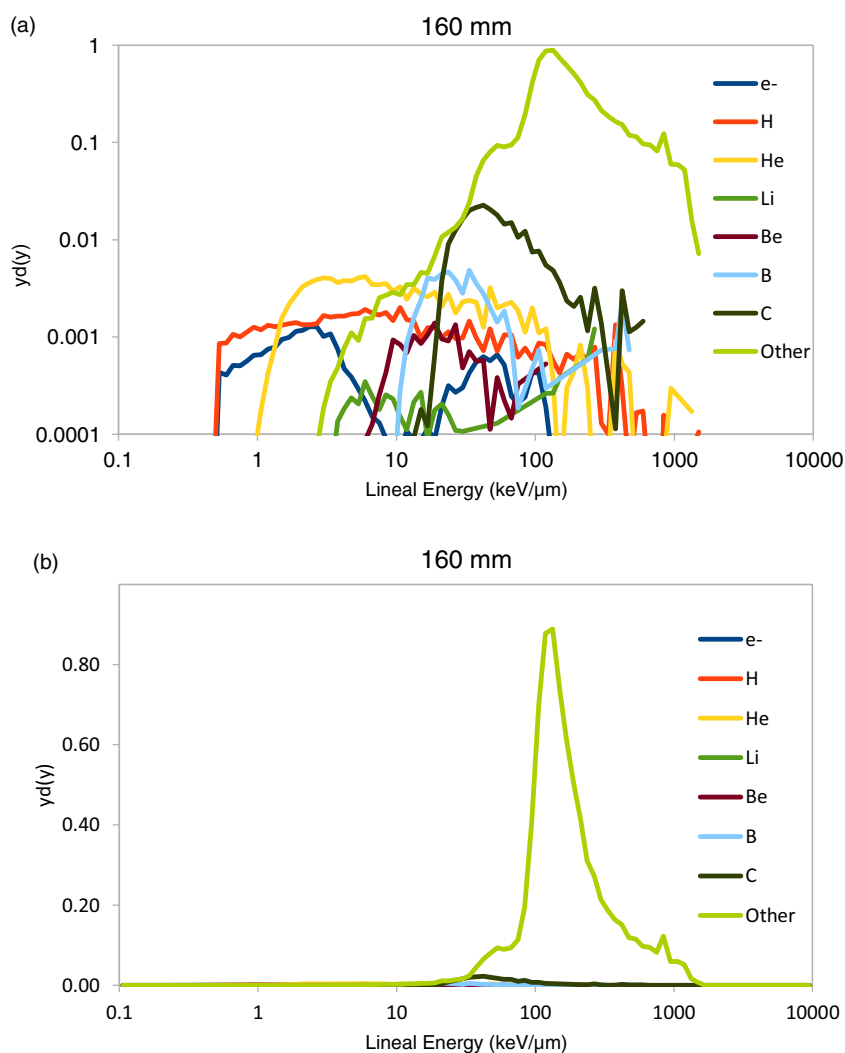


**Figure 16.** Secondary fragments contributing to the microdosimetric spectrum obtained with the Bridge SOI micropdosimeter for 345 MeV/u  $^{16}\text{O}$  ion beam set at 160 mm depth (a) log-log scale (b) semi-log scale

maximum  $\text{RBE}_{10}$  values of oxygen ions occurred at the same position as the maximum dose at the Bragg peak. This result was also slightly different from the measurement value in the literature, which occurred just before the maximum physical dose. This might be due to the fragmentation model accuracy in TOPAS simulation. Future improvement and verification are needed because of the importance of these quantities for accurate biological dose prediction.

With respect to carbon ions, oxygen ions produce higher nuclear fragmentations. Secondary fragments have a significant impact on the RBE, especially beyond the Bragg peak and out-of-field. The accuracy of fragmentation in the physical models used in CPT simulation is therefore of high importance. Further verification with experimental data of the physical models available in the Geant4 TOPAS is required.

These results also demonstrate that oxygen beams may have the advantage for cancer treatment because oxygen ions provide higher  $\text{RBE}_{10}$  values and have the same positions with the

maximum dose at the Bragg peak compared to carbon beams. These findings provide important information for accurate biological dose prediction, especially when targeting the tumours near organs at risk. The  $\text{RBE}_{10}$  of oxygen ions is higher than carbon ions in this work. These results are similar to the study by Tommasino et al. [5] using research treatment planning system and Tran et al. [9] using both Monte Carlo simulation and microdosimetry measurement performed at the Gunma University heavy-ion medical centre. This is because oxygen ions with higher Z numbers carrying higher charges would deposit higher doses than carbon ions and are translated into higher  $\text{RBE}_{10}$ .

However, the higher RBE values for oxygen ions at the entrance and in the distal part of the Bragg peak also result in higher toxicity for healthy tissues. Even though the RBE of oxygen ions is higher than the RBE of carbon ions around the Bragg Peak, where the tumour is located, the advantages and disadvantages of using oxygen ions are controversial issues. The study also presented a fast and reliable radiation field characterisation and RBE prediction

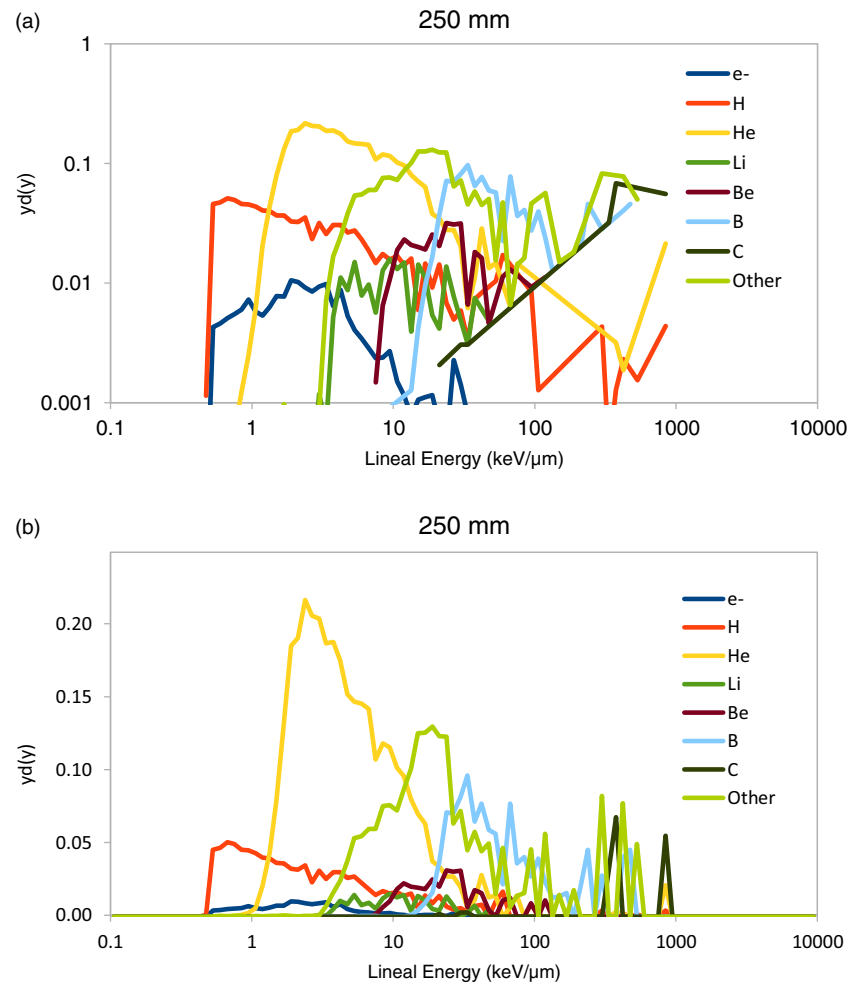


**Figure 17.** Secondary fragments contributing to the microdosimetric spectrum obtained with the Bridge SOI micrpdosimeter for 345 MeV/u <sup>16</sup>O ion beam set at 50 mm depth (a) log-log scale (b) semi-log scale

tool in CPT for heavy-ion beams using TOPAS-based simulations toolkit. The results of the study could support the commissioning of RBE used in treatment planning system and quality assurance.

**Acknowledgement.** This work was supported by Ministry of Higher Education Malaysia for Fundamental Research Grant Scheme (FRGS) with Project Code: FRGS/1/2019/STG02/USM/02/7. The author would like to thank Prof Anatoly Rosenfeld from Centre of Medical Radiation Physics, University of Wollongong for his guidance and support for the study.

## References

- Okada T, Kamada T, Tsuji H, et al. Carbon ion radiotherapy: clinical experiences at National Institute of Radiological Science (NIRS). *J Radiat Res* 2010; 51 (4): 355–364. <https://doi.org/10.1269/jrr.10016>
- Suit H, DeLaney T, Goldberg S, et al. Proton vs carbon ion beams in the definitive radiation treatment of cancer patients. *Radiother Oncol* 2010; 95 (1): 3–22. <https://doi.org/10.1016/j.radonc.2010.01.015>
- Schulz-Ertner D, Tsujii H. Particle radiation therapy using proton and heavier ion beams. *J Clin Oncol* 2007; 25 (8): 953–964. <https://doi.org/10.1200/jco.2006.09.7816>
- Amaldi U, Kraft G. Radiotherapy with beams of carbon ions. *Rep Prog Phys* 2005; 68 (8): 1861–1882. <https://doi.org/10.1088/0034-4885/68/8/r04>
- Tommasino F, Scifoni E, Durante M. New ions for therapy. *Int J Particle Therapy* 2015; 2 (3): 428–438. <https://doi.org/10.14338/ijpt-15-00027.1>
- Ying C, Bolst D, Rosenfeld A, Guatelli S. Characterization of the mixed radiation field produced by carbon and oxygen ion beams of therapeutic energy: a Monte Carlo simulation study. *J Med Phys* 2019; 44 (4): 263. [https://doi.org/10.4103/jmp.jmp\\_40\\_19](https://doi.org/10.4103/jmp.jmp_40_19)
- Scifoni E, Tinganelli W, Weyrather W K, Durante M, Maier A, Krämer M. Including oxygen enhancement ratio in ion beam treatment planning: model implementation and experimental verification. *Phys Med Biol* 2013; 58 (11): 3871–3895. <https://doi.org/10.1088/0031-9155/58/11/3871>
- Bassler N, Toftegaard J, Lühr A, et al. LET-painting increases tumour control probability in hypoxic tumours. *Acta Oncologica* 2013; 53 (1): 25–32. <https://doi.org/10.3109/0284186x.2013.832835>
- Tran L T, Bolst D, Guatelli S, et al. The relative biological effectiveness for carbon, nitrogen, and oxygen ion beams using passive and scanning techniques evaluated with fully 3D silicon microdosimeters. *Med Phys* 2018; 45 (5): 2299–2308. <https://doi.org/10.1002/mp.12874>
- Kraft G. Tumor therapy with heavy charged particles. *Prog Particle Nuclear Phys* 2001; 46 (2): 1. [https://doi.org/10.1016/s0146-6410\(01\)00151-x](https://doi.org/10.1016/s0146-6410(01)00151-x)
- Rosenfeld A B. Novel detectors for silicon based microdosimetry, their concepts and applications. *Nucl Instrum Methods Phys Res Sect A* 2016; 809: 156–170. <https://doi.org/10.1016/j.nima.2015.08.059>
- Perl J, Shin J, Schümann J, Faddegon B, Paganetti H. TOPAS: an innovative proton Monte Carlo platform for research and clinical applications. *Med Phys*, 2012; 39 (11): 6818–6837. <https://doi.org/10.1118/1.4758060>
- Faddegon B, Ramos-Méndez J, Schuemann J, et al. The TOPAS tool for particle simulation, a Monte Carlo simulation tool for physics, biology and

- clinical research. *Phys Med*, 2020; 72: 114–121. <https://doi.org/10.1016/j.jmp.2020.03.019>
14. Agostinelli S, Allison J, Amako K, et al. Geant4—a simulation toolkit. *Nucl Instrum Methods Phys Res Sect A Accel Spectrom Detect Assoc Equip* 2003; 506 (3): 250–303.
  15. Zhu H, Chen Y, Sung W, et al. The microdosimetric extension in TOPAS: development and comparison with published data. *Phys Med Biol* 2019; 64 (14): 145004. <https://doi.org/10.1088/1361-6560/ab23a3>
  16. Tran L T, Chartier L, Bolst D, et al. Characterization of proton pencil beam scanning and passive beam using a high spatial resolution solid-state microdosimeter. *Med Phys* 2017; 44 (11): 6085–6095. <https://doi.org/10.1002/mp.12563>
  17. Anon. Microdosimetry ICRU report 36. United States: International Commission on Radiation Units and Measurements, 1983.
  18. Kase Y, Kanai T, Matsumoto Y, et al. Microdosimetric measurements and estimation of human cell survival for heavy-ion beams. *Radiat Res* 2006; 166 (4): 629–638. <https://doi.org/10.1667/rr0536.1>
  19. Kase, Y., Yamashita, W., Matsufuji, N, et al. Microdosimetric calculation of relative biological effectiveness for design of therapeutic proton beams. *J Radiat Res* 2012; 54 (3): 485–493. <https://doi.org/10.1093/jrr/rrs110>
  20. Rossi H H, Zaider M. *Microdosimetry and Its Applications*. Springer Publishing, 2012.
  21. Bolst D, Guatelli S, Tran L T, et al. Correction factors to convert microdosimetry measurements in silicon to tissue in 12C ion therapy. *Phys Med Biol* 2017; 62 (6): 2055–2069. <https://doi.org/10.1088/1361-6560/aa5de5>
  22. Bolst D, Tran L T, Chartier L, et al. RBE study using solid state microdosimetry in heavy ion therapy. *Radiat Meas* 2017; 106: 512–518. <https://doi.org/10.1016/j.radmeas.2017.02.008>
  23. Tran LT, Chartier L, Bolst D, et al. 3D Silicon Microdosimetry and RBE study using 12C ion of different energies. *IEEE Trans Nucl Sci* 2015b; 62 (6): 3027–3033.
  24. Bradley P, Rosenfeld A, Lee K, Jamieson D, Heiser G, Satoh S. Charge collection and radiation hardness of a SOI microdosimeter for medical and space applications. *IEEE Trans Nuclear Sci* 1998; 45 (6): 2700–2710. <https://doi.org/10.1109/23.736518>
  25. Cornelius I, Rosenfeld A, Siegele R, Cohen D. LET dependence of the charge collection efficiency of silicon microdosimeters. *IEEE Trans Nuclear Sci* 2003; 50 (6): 2373–2379. <https://doi.org/10.1109/tns.2003.820740>
  26. Tran LT, Chartier L, Prokopovich D A. 3D-mesa “Bridge” silicon microdosimeter: charge collection study and application to RBE studies in 12C radiation therapy. *IEEE Trans Nucl Sci* 2015a; 62 (2): 504–511. <https://doi.org/10.1109/tns.2015.2391102>
  27. Torikoshi M, Minohara S, Kanematsu N, et al. Irradiation system for HIMAC. *J Radiat Res* 2007; 48 (Suppl A): A15–A25. <https://doi.org/10.1269/jrr.48.a15>
  28. Arce P, Bolst D, Bordage M, et al. Report on G4-Med, a Geant4 benchmarking system for medical physics applications developed by the Geant4 Medical Simulation Benchmarking Group. *Med Phys* 2020; 48 (1): 19–56. <https://doi.org/10.1002/mp.14226>
  29. Parisi G, Schettino G, Romano F. A systematic study of the contribution of counting statistics to the final lineal energy uncertainty in microdosimetry. *Phys Med Biol* 2022; 67 (15). <https://doi.org/10.1088/1361-6560/ac79fb>
  30. Rollet, S., Colautti, P., Grosswendt B, et al. Monte Carlo simulation of mini TEPC microdosimetric spectra: influence of low energy electrons. *Radiat Meas* 2010; 45: 1330–1333
  31. Conte V, Agosteo S, Bianchi A, et al. Microdosimetry of a therapeutic proton beam with a mini-TEPC and a MicroPlus-Bridge detector for RBE assessment. *Phys Med Biol* 2020; 65 (24): 245018. <https://doi.org/10.1088/1361-6560/abc368>